analytical chemistry

pubs.acs.org/ac Article

Simultaneous Native Mass Spectrometry Analysis of Single and Double Mutants To Probe Lipid Binding to Membrane Proteins

Hiruni S. Jayasekera, Farhana Afrin Mohona, Megan Ewbank, and Michael T. Marty*

Cite This: https://doi.org/10.1021/acs.analchem.4c01704 Read Online

ACCESS | Metrics & More | Article Recommendations | Supporting Information

ABSTRACT: Lipids are critical modulators of membrane protein structure and function. However, it is challenging to investigate the thermodynamics of protein−lipid interactions because lipids can simultaneously bind membrane proteins at different sites with different specificities. Here, we developed a native mass spectrometry (MS) approach using single and double mutants to measure the relative energetic contributions of specific residues on Aquaporin Z (AqpZ) toward cardiolipin (CL) binding. We first mutated potential lipid-binding residues on AqpZ, and mixed mutant and wild-type proteins together with CL. By using native MS to simultaneously resolve lipid binding to the mutant and wild-type proteins in a single spectrum, we directly determined the relative affinities of CL binding, thereby revealing the relative Gibbs free energy change for lipid binding caused by the mutation. Comparing different mutants revealed that W14 contributes to the tightest CL binding site, with R224 contributing to a lower affinity site. Using double mutant cycling, we investigated the synergy between W14 and R224 sites on CL binding. Overall, this novel native MS approach provides unique insights into the binding of lipids to specific sites on membrane proteins.

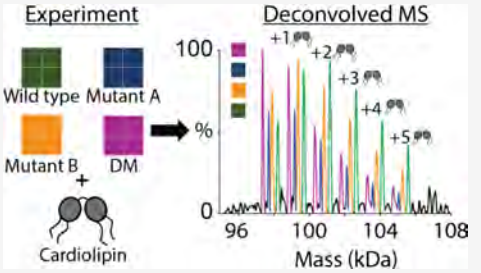

INTRODUCTION

Lipids can modulate the structure, function, and stability of membrane proteins through different types of interactions.[1−3] Indirectly, lipids can affect membrane proteins by changing the physical properties of the membrane, such as thickness or fluidity.[4−7] Conversely, lipids can also directly interact with specific sites on the membrane protein to modulate the stability and activity of the protein.[1,4−6,8,9] In between these two extremes, there is a sliding scale of specificities for lipids at different membrane protein binding sites, ranging from highly specific to totally nonspecific.[10,11] The diversity of lipid interactions makes it challenging to quantify the lipid binding affinity and selectivity at specific binding sites.

Native mass spectrometry (MS) has become a valuable tool for studying membrane protein−lipid interactions.[12−15] By using nondenaturing ionization conditions, native MS preserves folded structures and noncovalent interactions for mass analysis.[10,16−20] Moreover, native MS enables lipid interactions to be preserved in the gas-phase.[21−23] The ability of native MS to detect isolated membrane protein−lipid complexes has enabled measurement of lipid binding affinities and thermodynamics of protein−lipid interactions.[15,24−27] However, the conventional native MS approach requires multiple titrations with varying lipid concentrations, which is slow, laborious, and prone to errors. Unlike most other biophysical approaches, native MS can resolve small mass differences in a single spectrum, allowing lipid binding to be probed independently to any species that can be resolved in the mass spectrometer.[17,28,29] Leveraging this power, we developed a native MS experiment design to simultaneously examine the energetic contributions of selected amino acids to lipid binding by comparing wild-type and mutant proteins in the same spectrum. This single mutant approach directly reveals differences in lipid binding affinity caused by the mutations, enabling the ranking of lipid binding sites based on their thermodynamic trends.

Double mutant cycling was previously developed to determine the energetic coupling between amino acids in protein−ligand[30−32] and protein−protein interactions.[33−38] In a double mutant cycle, two different amino acid residues are mutated separately and in combination to create individual mutants and their corresponding double mutant.[33,35] The binding free energy is then measured for the wild type, each mutant, and the double mutant against each other. If the sum of the individual free energy changes for both single mutants relative to the wild type differs from the free energy change for the wild-type relative to the double mutant, the two residues are energetically coupled.[17,35,39] Coupling between residues is a separate concept from cooperativity in binding. Cooperativity refers to the binding of one ligand influencing the binding affinity of a second ligand, either positively or negatively. In contrast, coupling refers to how two residues bind a single

Received: April 1, 2024
Revised: May 22, 2024
Accepted: May 30, 2024

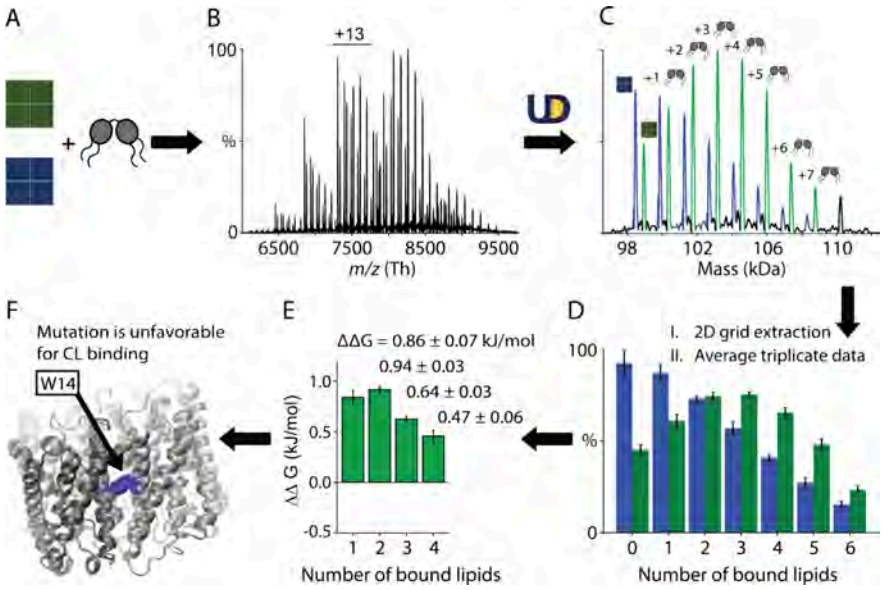

Figure 1. Schematic of single mutant analysis experiment and its data processing workflow. (A) Wild-type (WT) and W14A mutant proteins are mixed with CL at an approximate ratio of 1:1:100 of WT:W14A:CL. Wild type and W14A are annotated as tetrameric squares colored in *green* and *blue*, respectively, and CL is represented in a *gray* graphic. (B) Raw and (C) deconvolved mass spectra for a representative replicate at 25 °C for the wild type and mutant proteins with a series of lipids bound where deconvolved peaks are colored in *green* and *blue*, respectively. The number of lipids bound is annotated. Each peak area was extracted, and (D) the bar chart shows the average and standard deviation from the three replicate measurements. Calculated from eq 3, (E) the differences in the Gibbs free energy change ($\Delta\Delta G$) plot for binding of up to four lipids reveal that (F) the W14A mutation is unfavorable for CL binding. The W14 site on one monomer is annotated in blue while the entire protein complex is *gray*.

ligand, either working together to promote binding or working in opposition. A system with a single binding site can have coupling but cannot have cooperativity. Systems with multiple binding sites can have both, but here, we have focused exclusively on coupling.

Previous work by Horovitz and Sharon has used native MS to examine protein−protein interactions through double mutant cycle analysis.[37] Because its high resolution can distinguish distinct masses of all the mutants, native MS provides a powerful advance of the method by enabling simultaneous detection of all interactions from a single spectrum.[37] Here, we apply native MS to extend double mutant cycling to study the coupling between amino acid residues for membrane protein−lipid interactions.

We applied these advanced experiments to study the binding of cardiolipin (CL) (Figure S1) to aquaporin Z (AqpZ). AqpZ, a homotetramer, is responsible for the selective, passive transport of water across membranes.[40−43] Previous work has shown that CL binds to AqpZ and affects its activity.[44,45] A prior study by Schmidt and co-workers investigated a mutation that disrupted CL binding using native MS and molecular dynamic simulations, which proposed CL binding sites at the monomer−monomer interface of AqpZ.[44−46] However, it remains challenging to measure the affinity and thermodynamics of binding of CL to AqpZ.

Here, we measured the thermodynamic contributions of a range of amino acid residues to AqpZ−CL interactions using native MS on mixtures of AqpZ wild type, single mutants, or double mutants bound to CL. Our data revealed the relative change in the binding free energy caused by mutating specific residues on multiple CL-bound states. Moreover, double mutant cycle analysis revealed energetic coupling between two residues for CL binding.

THEORY

We begin by considering the dissociation of a protein−lipid complex, *PL*, into free protein, *P*, and free lipid, *L*: $PL \rightleftharpoons P + L$. We can write a conventional expression for the dissociation constant, K_D:

$$K_D = \frac{[P] \times [L]}{[PL]} \tag{1}$$

Using the conventional approach, if we assume that *P* and *PL* have similar detector responses, we can use native MS to measure the ratio of the signal intensities of *P* and *PL* from a single spectrum, but multiple spectra are usually collected to fit the unknown free lipid term, *L*, with higher accuracy.[20,47−49] To compare the relative affinities of mutant and wild-type proteins using this approach, multiple titration series[32] would have to be performed with each protein independently, increasing the time, labor, and potential for experimental errors.

Here, we developed an alternative approach to directly measure the relative binding affinities of two species from a single spectrum. First, both wild-type (*W*) and mutant (*M*) proteins are mixed with lipids in a single tube to form *WL* and *ML* complexes. Because all of the species are present in the same solution, the free lipid term, *L*, will be identical for both species. Thus, we can express the relative affinities of the wild-type ($K_{D,w}$) and mutant ($K_{D,M}$) protein as a ratio, *K*, that cancels out the free lipid term:

$$K = \frac{K_{D,W}}{K_{D,M}} = \frac{[W] \times [L]}{[WL]} \times \frac{[ML]}{[M] \times [L]} = \frac{[W] \times [ML]}{[WL] \times [M]} \tag{2}$$

As noted above, we assume that the native MS signal intensities are proportional to concentration for all terms in

https://doi.org/10.1021/acs.analchem.4c01704
Anal. Chem. XXXX, XXX, XXX−XXX

this equation. Thus, as described in the Supporting Methods, we calculate the native MS peak areas for each signal and subsitute these into eq 2 in place of concentration values. This ratio of dissociation constants for the *WL* and *ML* complexes is also the equilibrium constant for the exchange of a lipid between the mutant and wild type, $WL + M \rightleftharpoons W + ML$. Up to this point, we have focused on a single lipid binding the apo protein, but similar equations can be written for binding of a second lipid to a complex with one lipid bound, binding a third lipid to a complex with two lipids, and so on.

Importantly, native MS can distinguish the wild-type and mutant proteins with different numbers of bound lipids in the same spectrum (Figure 1C and 2B), providing direct measurements of all terms in eq 2 without the need for multiple titrations. This experimental design also has several inherent internal controls that limit experimental errors. Specifically, small errors in the lipid concentration are internally controlled, because everything is combined in a single tube. Similarly, small errors in the protein concentrations do not factor into the equation, because only the ratio of bound and unbound for each species is used.

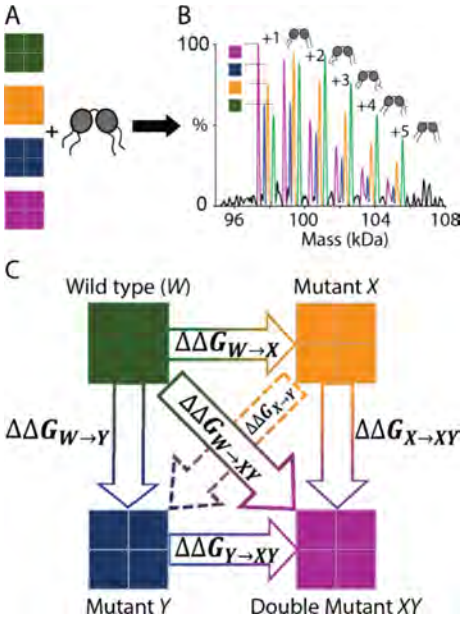

Figure 2. Schematic of the double mutant cycle experiment and its data processing workflow. (A) Wild-type and mutant proteins (*X*, *Y*, and *XY*) are mixed with CL at an approximate ratio of 1:1:1:1:200, where the proteins are represented in tetrameric squares colored in *green*, *yellow*, *blue*, and *purple*, respectively, and CL is represented in a *gray* graphic. (B) Deconvolved mass spectra independently resolve all four proteins, indicated in their respective colors. The numbers of bound lipids are annotated. (C) Extraction and pairwise comparison of the relative peak areas for each bound lipid enable the construction of the double mutant cycle.

From the equilibrium constant for the exchange of a lipid between the mutant and the wild-type forms, we can derive an expression for the difference in the Gibbs free energy change for lipid binding between wild type and mutant, $\Delta\Delta G$ as

$$\Delta\Delta G = -RT \ln K = -RT \ln \frac{[W] \times [ML]}{[WL] \times [M]} \quad (3)$$

where R is the ideal gas constant, T is the temperature in Kelvin, and K is the equilibrium constant from eq 2. The $\Delta\Delta G$ indicates how favorable CL binding is to the mutant relative to the wild type. Positive values (Figure 1E) show that the mutation is less favorable for CL binding to the mutant relative to the wild type, and negative values indicate that the mutant is more favorable for CL binding. Therefore, the $\Delta\Delta G$ values quantify how much each residue contributes to CL binding relative to that of the mutant form.

It is important to note that AqpZ is a homotetramer and each mutation will thus affect four symmetric binding sites. Moreover, there are multiple sites where lipids can bind, which we have not tried to model. Thus, these $\Delta\Delta G$ values do not measure a single lipid binding a single site. Rather, they represent the relative global binding affinities averaged across multiple sites and are most useful when considering the overall trends rather than absolute energies. For simplicity, we have also not tried to examine lipid cooperativity but instead simply report results for binding of each lipid.

Combining sets of data for individual mutants with their double mutants to construct a double mutant cycle reveals coupling interactions between residues during lipid binding. However, comparing data from single mutant analyses performed in separate tubes for each mutant with those of the wild type did not provide accurate energy differences, potentially because the protein mixing ratios and free lipid concentrations could vary between experiments. To overcome this limitation, we carried out a separate experiment with four proteins—wild type (*W*), mutant *X*, mutant *Y*, and the double mutant (*XY*)—in the same tube to construct the double mutant cycle (Figure 2).

For independent residues in this cycle that are not coupled, the $\Delta\Delta G$ for a single mutation should be identical, regardless of whether the other mutation has been made: $\Delta\Delta G_{W\rightarrow X} - \Delta\Delta G_{Y\rightarrow XY} = \Delta\Delta G_{W\rightarrow Y} - \Delta\Delta G_{X\rightarrow XY} = 0$ (Figure 2C). A nonzero value indicates that there is an interaction or energetic coupling between the two mutated residues.[50] Coupling can also be observed by comparing the free energies associated with the double mutant against the sum of independent free energies of individual mutants. In an uncoupled system, $\Delta\Delta G_{W\rightarrow XY} = \Delta\Delta G_{W\rightarrow X} - \Delta\Delta G_{W\rightarrow Y}$ (Figure 2C).[39] In other words, if the double mutant is not equal to the sum of the parts, then the two residues are coupled.

EXPERIMENTAL SECTION

Mutant Selection and Mutagenesis. A previous molecular dynamics simulation study on Aquaporin Z (AqpZ) by Schmidt et al. found that CL tends to associate at the interface between monomers, and the occupancy of CL around AqpZ was reduced when W14 was mutated to alanine.[44] Therefore, we selected W14A as the first mutant. To further identify the specific CL binding sites, we chose positively charged arginine and lysine residues near the monomer−monomer interface, specifically R75, R224, and K4 because CL is anionic (Figure S1). We predicted that CL might interact with these cationic residues. Selected residues were mutated to alanine through site-directed mutagenesis to create single mutants W14A, R224A, R75A, and K4A and double mutants R224A_R75A and R224A_W14A (see Figure 3). Purified AqpZ-TEV-GFP-HIS proteins were cleaved with tobacco etch virus (TEV) protease and then purified by immobilized metal affinity chromatography followed by the buffer exchange into 200 mM ammonium acetate buffer with

https://doi.org/10.1021/acs.analchem.4c01704
Anal. Chem. XXXX, XXX, XXX−XXX

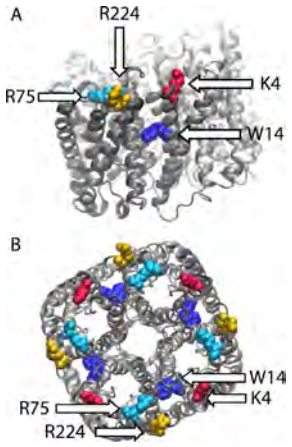

Figure 3. (A) Side-view and (B) top-view of AqpZ with mutant sites W14, R224, R75, and K4 labeled, indicated with an arrow, and colored *blue*, *yellow*, *cyan*, and *red*, respectively. Four chains of the protein are shown in *gray*. PDB code: 2abm.[53]

0.5% tetraethylene glycol monooctyl ether (C8E4) using size exclusion chromatography with a Superose 6 10/300 Increase GL (Cytiva). More details on mutagensis, protein expression, and purification can be found in Supporting Methods.

Native MS Sample Preparation and Analysis. 1′,3′-Bis[1-palmitoyl-2-oleoyl-*sn*-glycero-3-phospho]-glycerol (sodium salt) (16:0−18:1 CL) was purchased from Avanti Polar Lipids, dissolved in chloroform, quantified using phosphate analysis, and dried under N_2 gas and vacuum overnight.[44,45] A stock concentration of 1.5 mM CL was prepared in 200 mM ammonium acetate buffer with 0.5% C8E4, as previously described.[44] We performed another phosphate analysis on the stock CL prepared to confirm the exact concentration.

For the single mutant experiment, pairwise combinations of wild type with single mutants and double mutants were mixed, and CL was added to each before incubation at 4 °C for 15−30 min. Longer incubation times of 3 h and overnight were comparable with those at 15 min, indicating the system was at equilibrium. Membrane proteins were mixed in a roughly 1:1 molar ratio, but this ratio was slightly adjusted for each pair to achieve approximately equal MS signals for the two proteins. We used a ratio of approximately 1:1:100 protein A:protein B:CL, but the CL ratio was slightly adjusted to a range of 100−120 to achieve a spectral density of 6−7 bound lipids, which allowed us to measure multiple lipid-bound states.

For double mutant cycle analysis of two high-affinity amino acid residues, we mixed AqpZ wild type, R224A, W14A, and their corresponding double mutant (DM) at an approximately 1:1:1:1 ratio. This ratio was slightly adjusted to achieve approximately equal MS signals for all proteins. Then, we added CL prior to the incubation at 4 °C for 15−30 min to achieve an approximate ratio of 1:1:1:1:200 WT:R224A:W14A:DM:CL to obtain 5−6 bound lipids. To observe the concentration dependence, we also performed double mutant cycle experiments at lower CL ratios of 1:1:1:1:100, 1:1:1:1:50, and 1:1:1:1:25.

Native MS of the samples was performed using a Q-Exactive HF Orbitrap mass spectrometer (Thermo Fisher Scientific, Bremen) equipped with a variable temperature (VT) source[51] in positive ion mode. Key MS settings included a mass range of 2000−25000 m/z for single mutant analysis and 4000−15000 m/z for double mutant cycle analysis, resolution at 15,000, 1.10−1.15 kV capillary voltage, 200 °C capillary temperature, 50−60 V source fragmentation, 80−95 V collision voltage, and trapping gas pressure setting of 7. Higher collision voltages did not cause significant loss of bound lipids, incidating that the lipid binding was stable in the gas phase (Figure S2). Additional details are provided in the Supporting Methods. Upon placing the needle inside the VT source, the sample was allowed to equilibrate to the set temperature for 2 min. Once the sample was equilibrated, mass spectra were acquired at the set temperature for 1.5 min. Similarly, spectra were acquired at temperatures ranging from 15 to 35 °C at 5 °C intervals.

To verify that AqpZ subunits with different mutants do not mix to form hybrid complexes (such as a tetramer complex with two mutant and two wild-type monomers), we mixed the wild-type and double mutant proteins without lipid and checked the mass spectrum over time. If subunit exchange were occurring, we would expect to see heterogeneous species with unique masses appearing in between the two homogeneous starting peaks. Instead, even after an overnight incubation at 4 °C, there was no evidence of subunit exchange (Figure S3). Nonetheless, it is advisible not to prolong incubation times for longer than necessary, as this may result in protein degradation and/or subunit exchange.

MS data analysis was performed using UniDec[52] and custom Python scripts. Full details are provided in Supporting Methods.

RESULTS AND DISCUSSION

Single Mutant Analysis. First, we investigated the thermodynamics of CL binding to different potential lipid binding sites on AqpZ by measuring simultaneous lipid binding to wild-type and mutant proteins using native MS. We began with the W14A mutation, which sits at the monomer interface (Figure 3) and was suggested to be involved in CL binding.[43,44,46] After incubating the wild type and W14A mutant with CL, we performed native MS. In the spectra (Figure 1B, 1C, and S4), we observed a peak series for the wild-type and mutant proteins with the mutant slightly lower in mass (Table S1). Within each peak series, distinct peaks were observed for up to 7 bound CL molecules, with each peak separated by the mass of CL.

Globally, the peak series is clearly shifted toward lower lipid binding with the W14A mutant relative to the wild type (Figure 1C), which suggests a lower affinity of the mutant for CL binding. To quantify the relative affinity difference for each bound lipid, we calculated the equilibrium constant for lipid exchange between the mutant and wild type (eq 2), and we used this value to calculate the change in Gibbs free energy for lipid binding caused by the mutation (eq 3).

The positive $\Delta\Delta G$ values for each of the first four bound lipids (Table S2 and Figure 4A) indicate that CL binding is less favorable to the W14A mutant than that to the wild type. In other words, the W14 residue contributes an average of about 0.86 kJ/mol to the global binding of the first CL, relative to an alanine in the same location. Interestingly, the effect was most pronounced when comparing 0 vs 1 and 1 vs 2 bound lipids. Comparing states with higher amounts of bound lipids, such as 2 vs 3, we see positive $\Delta\Delta G$ values but with decreasing magnitudes. When comparing even higher amounts of lipids bound, such as 4 vs 5 and 5 vs 6, the values continue to decrease, but confidence intervals increase at higher values due to the weaker signals (Figure S5). Although these are relatively

https://doi.org/10.1021/acs.analchem.4c01704
Anal. Chem. XXXX, XXX, XXX−XXX

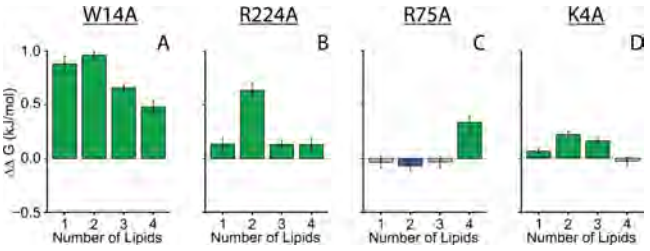

Figure 4. Difference in the Gibbs free energy change ($\Delta\Delta G$ plots) for CL binding up to four lipids at 25 °C for each mutant (A) W14A, (B) R224A, (C) R75A, and (D) K4A compared to the wild-type protein. Error bars indicate the 95% confidence intervals. Green bars represent unfavorable mutations, where CL binding is more favorable to the wild type. Negative blue bars depict more favorable CL binding to the mutant. Gray bars represent statistically insignificant interactions.

small changes in ΔG, they clearly disrupt the global profile of lipid binding observed by native MS, as seen in Figure S4.

These data indicate that W14 either participates directly in a binding site for CL or plays an indirect role in the binding of CL to another site on AqpZ. Our interpretation for the observed decrease in $\Delta\Delta G$ as more lipids bind is that the binding site involving W14 has the strongest affinity for CL, out of the residues studied here. If only one CL is bound (comparing 0 vs 1), W14 makes a strong contribution to lipid binding at this higher affinity site. Because AqpZ is a homotetramer, there are 4 potential binding sites that involve W14. As additional lipids bind (1 vs 2, 2 vs 3, etc.), they can bind at the other open symmetric sites involving W14. However, they can also bind at different sites, due in part to their being fewer open binding sites involving W14 to access. Because these other binding sites are not probed by the W14A mutation, the W14A mutation has a lower contribution to the global free energy of lipid binding as more lipids are bound in more diverse sites.

After examining W14, we next explored surface exposed positively charged amino acids near the monomer interfaces of AqpZ. We started with the R224A mutant (Figure 3). We performed a single mutant analysis with wild-type and R224A mutant proteins mixed with CL. Like W14A, we observed distinct peak series for the wild-type and R224A proteins with up to 7 lipids bound (Figure S4), and we calculated positive $\Delta\Delta G$ values (Table S2 and Figure 4B), which indicates that CL binding was also less favorable to the R224A mutant than the wild type.

However, the $\Delta\Delta G$ values for R224A were lower than the values for W14A, revealing a higher overall CL binding affinity for sites involving W14 over sites involving R224. Interestingly, for wild type and R224A, the highest $\Delta\Delta G$ value was for the second lipid binding (1 vs 2 bound lipids). Building on our interpretation of the W14A data discussed above, we interpret this pattern to indicate that the site involving R224 is the second highest affinity site for CL binding on AqpZ. When the first CL binds (0 vs 1), it primarily binds the site involving W14. When the second lipid binds (1 vs 2), it can bind at either one of the three open sites involving W14 or one of the four open sites involving R224. Although the W14 site is preferred, as evidenced by the statistically higher (p-value < 0.0001) $\Delta\Delta G$ between 1 vs 2 CL bound for W14A relative to R224A, there is still a significant population of lipids that bind at the R224 site after the first W14 site is occupied (compare lipid 2 in Figure 4A and B).

We then explored the R75 residue, which is close to R224 on the surface of AqpZ near the monomer interface (Figure 3). Single mutant analysis reveals that this mutant binds CL with an affinity slightly higher than that of the wild type, as evidenced by the negative $\Delta\Delta G$ value (Table S2 and Figure 4C). However, these data indicate that the R75 site does not contribute as much to CL binding. We only discovered a meaningful $\Delta\Delta G$ when comparing 3 vs 4 bound lipids. This observation suggests that the R75 residue is not important until at least 3 lipids are already bound to the complex, likely at the higher affinity sites involving W14 and R224.

Finally, we tested the K4 residue on the opposite side of the monomer interface from R224 (Figure 3). We performed a single mutant analysis between the wild-type protein and the K4A mutant in the same manner. K4A exhibited only minor effects on CL binding, with statistically positive but very low $\Delta\Delta G$ values. Thus, the K4 residue does not contribute much to CL binding.

R224 and R75 are close to each other, so we wanted to compare the wild-type protein and the double mutant of R224A and R75A. Like the R224A mutant, the double mutant also exhibited lower CL binding at the second bound lipid, with the highest $\Delta\Delta G$ value for 1 vs 2 bound lipids (Table S2 and Figure S6). These results more closely resembled those of the R224A mutant, confirming that the R224 residue has a stronger contribution to CL binding than R75.

Overall, our single mutant analyses indicate that W14 contributes to the highest affinity lipid binding site with R224 contributing to a second high affinity binding site. R75 contributes to CL binding only after several lipids are already bound, indicating a weak affinity, and K4 does not contribute much overall. Together, these data reveal multiple potential binding sites for CL around AqpZ and allow us to rank the binding sites based on the trends in their relative affinities.

Double Mutant Cycle Analysis. Based on our single mutant analysis, we propose that the W14 and R224 sites contribute to the highest and second highest affinity binding sites on AqpZ, respectively. To understand whether the binding of CL to one site (W14) influences the binding of CL to the other site (R224), we used double mutant cycle analysis, which allows us to explore the energetic coupling between residues.[17,33,35−37,39]

For the double mutant cycle experiment, we mixed all four proteins (wild-type, W14A, R224A, and R224A_W14A) in the same tube (Figure 2A). We observed resolved peaks with up to 5−6 bound lipids in all four proteins (Figure 2B−C and Figure S7). Comparing the $\Delta\Delta G$ plots obtained for wild-type with single mutant analysis (Figure 4A−B and Table S2) and the double mutant cycle experiment (Figure S7D−E and Table S3), we observed consistent patterns for the CL binding. However, there are slight differences in the values, potentially due to differences in free lipid concentrations and protein mixing ratios between experiments as well as the presence of 4 different proteins in the double mutant cycle experiment mixture.

We constructed the double mutant cycles for binding of each of the first four lipids by a pairwise comparison of each species (Figure S8). However, we focused on the first two bound lipids (0 vs 1 and 1 vs 2) because those were most affected by these mutations (Figure 5). In both cases, the W14A mutation had a more pronounced effect on CL binding than the R224A mutation, with the left side greater than the top side of the box. We can directly quantify the difference in

https://doi.org/10.1021/acs.analchem.4c01704
Anal. Chem. XXXX, XXX, XXX−XXX

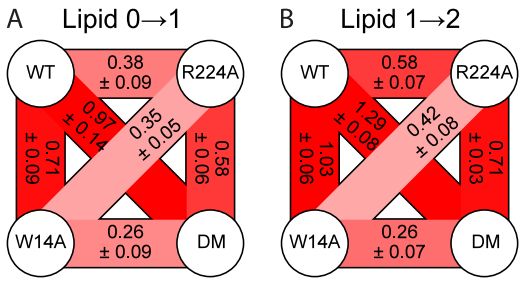

Figure 5. Double mutant cycle for the (A) first and (B) second CL bindings constructed with AqpZ WT, R224A, W14A, and R224A_W14A (DM) at 25 °C. The mean $\Delta\Delta G$ in kJ/mol with ±95% confidence intervals are stated. Positive $\Delta\Delta G$ values are depicted in darker *red* for higher values. Data from lipids 2 to 3 and 3 to 4 can be found in Figure S8C−D, respectively.

effects of the two mutants by comparing the upward diagonal between W14A and R224A. Here, we found that the W14A was 0.35 ± 0.05 kJ/mol more disruptive than R224A for the first CL binding and 0.42 ± 0.08 more disruptive for the second CL (Figure 5).

To investigate coupling between the W14 and R224 residues, we compared the $\Delta\Delta G$ values associated with the double mutant and the individual mutants. If the selected mutants are energetically independent, $\Delta\Delta G$ for the double mutant would be the sum of the $\Delta\Delta G$ values for the individual mutants: $\Delta\Delta G_{W\rightarrow XY} = \Delta\Delta G_{W\rightarrow X} + \Delta\Delta G_{W\rightarrow Y}$ (Figure 2C). In simpler terms, the diagonal of the box in Figure 5A would be equal to the sum of the top and left sides if the residues were independent. For the first bound lipid (0 vs 1), we discovered that the $\Delta\Delta G$ between the wild type and double mutant (0.97 ± 0.14 kJ/mol) was statistically equal to the sum of the individual mutants (1.09 ± 0.13 kJ/mol), indicating independent CL binding at each site.

Similarly, independent free energies should show the same $\Delta\Delta G$ for the same mutation regardless of whether the other residue has been mutated. In other words, opposite sides of the box in Figure 5A should be equal if the residues are independent. For the first bound lipid (0 vs 1), we found that the differences in $\Delta\Delta G$ values between the top arm vs bottom for the R224A mutation (0.12 ± 0.12 kJ/mol) and the right arm vs left for the W14A mutation (0.13 ± 0.11 kJ/mol) were small, indicating again that these sites do not appear to interact for the first lipid binding at high concentrations.

However, for the second lipid binding on AqpZ (Figure 5B), the two residues were not independent but instead couple. The diagonal comparing the double mutant to the wild type (1.29 ± 0.08 kJ/mol) was not equal to the sum of the individual mutants (1.61 ± 0.09 kJ/mol). Instead, the double mutant was lower than the sum of the two single mutants, indicating a coupling energy, $CE = \Delta\Delta G_{W\rightarrow XY} - (\Delta\Delta G_{W\rightarrow X} + \Delta\Delta G_{W\rightarrow Y})$, of −0.32 ± 0.12 kJ/mol between the W14 and R224 residues for CL binding, relative to alanines at the same locations. Coupling was also evident when considering the two opposing sides of the box (top and bottom or right and left), which showed a difference of around 0.32 kJ/mol between each pair of arms.

To determine whether the coupling is positive or negative, we considered the change in CL binding from each mutation. The impact of the W14A mutation was −0.32 ± 0.07 kJ/mol less impactful when the R224A mutation was already present (right arm < left arm). This difference shows that the W14A mutation was less detrimental to CL binding if the R224A mutation was already made. Similarly, the R224A mutation was −0.32 ± 0.10 kJ/mol less impactful when the W14A mutant was already made (bottom arm < top arm). Because the effect of one mutation became less pronounced when the other mutation was present, the presence of both residues is more favorable to CL binding than expected from each single residue, a positive synergy in binding CL. Therefore, R224 and W14 work together to promote CL binding to AqpZ.

Finally, we investigated the concentration dependence of these changes by varying the membrane protein:lipid ratio. At lower CL concentrations, there were not enough lipids to detect three or four bound lipids (Figure S9 and Table S3). However, for the first and second bound lipids, the W14A mutation became more dominant than R224A (Figures S10 and S11). These data confirm that R224 contributes to a lower affinity binding site that is less occupied at lower concentrations than the higher affinity site involving W14.

Interestingly, the coupling between W14 and R224 was stronger for the first lipid at lower concentrations, despite the lower independent contributions from R224 (Figures S10 and S11 and Table S3). Our interpretation is that the R224 residue can contribute weakly to promote CL binding at the high affinity site. These contributions are entirely dependent on the presence of W14, as evidenced by the negligible differences between the double mutant and the W14A mutant. In other words, when W14 is mutated, R224 no longer contributes. At higher concentrations, this coupling is less prominent because other lower affinity binding sites can be populated, including a lower affinity site with independent R224 contributions. At lower concentrations, only the high affinity binding site is probed, so coupling may be more easily detected.

From a structural perspective, these data indicate that there is a higher affinity for the CL binding site involving W14. R224 weakly contributes to this higher affinity binding site in a manner that is entirely dependent on the presence of W14. However, R224 can also contribute independently to a lower affinity binding site that becomes more occupied at higher concentrations. It is not clear if coupling energies observed for the second bound lipid also indicate that binding of an initial CL at the higher affinity W14 site promotes binding of second CL at the lower affinity site involving independent R224 (intersite coupling). In any case, our results reveal that membrane protein residues can work together to facilitate the binding of lipid to membrane proteins.

CONCLUSION

To study the contributions of specific residues to the thermodynamics of membrane protein−lipid interactions, we used native MS to simultaneously measure the binding of lipids to a pair or quartet of membrane protein mutants. We simultaneously determined the relative binding affinities of CL to both wild type and single mutants, which enabled us to identify W14 as contributing to the highest affinity binding site and R224 as contributing to the second highest affinity binding site. In contrast, the R75 and K4 sites do not play a major role in binding to CL.

To investigate coupling interactions between W14 and R224 residues through double mutant cycling, we simultaneously mixed all four proteins: wild-type, two single mutants, and their corresponding double mutant. Interestingly, we observed a positive coupling interaction between the two residues for CL binding.

https://doi.org/10.1021/acs.analchem.4c01704
Anal. Chem. XXXX, XXX, XXX−XXX

In contrast to other techniques, native MS with mutant analyses offers a simple method for comparing thermodynamics of intermolecular interactions from a single spectrum.[37] Future work will explore thermodynamic parameters such as enthalpy and entropy through van't Hoff analysis, which unfortunately was not achievable in this study.[15] It may also be possible to build on these experiments to extract more complex information about the affinities of individual microscopic binding sites and lipid binding cooperativity. Although our simple binding model does not capture all of the complexity of lipid binding to membrane protein surfaces, this method provides valuable insights into understanding membrane protein−lipid interactions. Specifically, the trends in binding help to rank binding sites by their relative affinities and binding patterns. The measurements also reveal the presence and direction of the coupling.

■ ASSOCIATED CONTENT

Supporting Information

The Supporting Information is available free of charge at https://pubs.acs.org/doi/10.1021/acs.analchem.4c01704.

Supplemental methods on mutagenesis, protein expression, purification, and MS data analysis; supplemental tables with data analysis results; and supplemental figures with raw, deconvolved MS spectra, processed data, and double mutant cycles analysis data. All raw data for this manuscript is available at MassIVE (DOI: doi:10.25345/C53R0Q44F). (PDF)

■ AUTHOR INFORMATION

Corresponding Author

Michael T. Marty − *Department of Chemistry and Biochemistry and Bio5 Institute, University of Arizona, Tucson, Arizona 85721, United States;* orcid.org/0000-0001-8115-1772; Email: mtmarty@arizona.edu

Authors

Hiruni S. Jayasekera − *Department of Chemistry and Biochemistry and Bio5 Institute, University of Arizona, Tucson, Arizona 85721, United States*

Farhana Afrin Mohona − *Department of Chemistry and Biochemistry and Bio5 Institute, University of Arizona, Tucson, Arizona 85721, United States*

Megan Ewbank − *Department of Chemistry and Biochemistry and Bio5 Institute, University of Arizona, Tucson, Arizona 85721, United States*

Complete contact information is available at: https://pubs.acs.org/10.1021/acs.analchem.4c01704

Notes

The authors declare no competing financial interest.

■ ACKNOWLEDGMENTS

The authors thank Maria Reinhardt-Szyba, Kyle Fort, and Alexander Makarov at Thermo Fisher Scientific for support on the Q-Exactive HF UHMR instrument. We also thank Professors Amnon Horovitz, Michal Sharon, and attendees at the Advancing Mass Spectrometry Conference 2023 for their constructive remarks and insights. This work was funded by the National Institutes of Health (NIH) under grant numbers R35 GM128624 and RM1 GM145416 to M.T.M.

■ REFERENCES

(1) Hunte, C. *Biochem. Soc. Trans.* **2005**, *33* (5), 938−942.
(2) Keener, J. E.; Jayasekera, H. S.; Marty, M. T. *Anal. Chem.* **2022**, *94* (23), 8497−8505.
(3) Levental, I.; Lyman, E. *Nat. Rev. Mol. Cell Biol.* **2023**, *24* (2), 107−122.
(4) Corradi, V.; Sejdiu, B. I.; Mesa-Galloso, H.; Abdizadeh, H.; Noskov, S. Yu.; Marrink, S. J.; Tieleman, D. P. *Chem. Rev.* **2019**, *119* (9), 5775−5848.
(5) Lee, A. G. *Biochim. Biophys. Acta BBA - Biomembr.* **2003**, *1612* (1), 1−40.
(6) Hunte, C.; Richers, S. *Curr. Opin. Struct. Biol.* **2008**, *18* (4), 406−411.
(7) Lee, A. G. *Mol. Biosyst.* **2005**, *1* (3), 203−212.
(8) Marius, P.; de Planque, M. R. R.; Williamson, P. T. F. *Biochim. Biophys. Acta* **2012**, *1818* (1), 90−96.
(9) Lee, A. G. *Biochim. Biophys. Acta BBA - Biomembr.* **2004**, *1666* (1), 62−87.
(10) Landreh, M.; Marty, M. T.; Gault, J.; Robinson, C. V. *Curr. Opin. Struct. Biol.* **2016**, *39*, 54−60.
(11) Yeagle, P. L. *Biochim. Biophys. Acta BBA - Biomembr.* **2014**, *1838* (6), 1548−1559.
(12) Bolla, J. R.; Agasid, M. T.; Mehmood, S.; Robinson, C. V. *Annu. Rev. Biochem.* **2019**, *88* (1), 85−111.
(13) van Duijn, E. *J. Am. Soc. Mass Spectrom.* **2010**, *21* (6), 971−978.
(14) Webb, I. K. *Biochim. Biophys. Acta BBA - Proteins Proteomics* **2022**, *1870* (1), 140732.
(15) Cong, X.; Liu, Y.; Liu, W.; Liang, X.; Russell, D. H.; Laganowsky, A. *J. Am. Chem. Soc.* **2016**, *138* (13), 4346−4349.
(16) Keener, J. E.; Zhang, G.; Marty, M. T. *Anal. Chem.* **2021**, *93* (1), 583−597.
(17) Horovitz, A.; Fleisher, R. C.; Mondal, T. *Curr. Opin. Struct. Biol.* **2019**, *58*, 10−17.
(18) Chandler, S. A.; Benesch, J. L. *Curr. Opin. Chem. Biol.* **2018**, *42*, 130−137.
(19) Mehmood, S.; Allison, T. M.; Robinson, C. V. *Annu. Rev. Phys. Chem.* **2015**, *66* (1), 453−474.
(20) Krishnaswamy, S. R.; Williams, E. R.; Kirsch, J. F. *Protein Sci.* **2006**, *15* (6), 1465−1475.
(21) Kundlacz, T.; Schmidt, C. *Anal. Chem.* **2023**, *95* (47), 17292−17299.
(22) Landreh, M.; Costeira-Paulo, J.; Gault, J.; Marklund, E. G.; Robinson, C. V. *Anal. Chem.* **2017**, *89* (14), 7425−7430.
(23) Qiao, P.; Liu, Y.; Zhang, T.; Benavides, A.; Laganowsky, A. *Biochemistry* **2020**, *59* (22), 2089−2099.
(24) Cong, X.; Liu, Y.; Liu, W.; Liang, X.; Laganowsky, A. *Nat. Commun.* **2017**, *8* (1), 2203.
(25) Qiao, P.; Schrecke, S.; Walker, T.; McCabe, J. W.; Lyu, J.; Zhu, Y.; Zhang, T.; Kumar, S.; Clemmer, D.; Russell, D. H.; Laganowsky, A. *J. Phys. Chem. Lett.* **2021**, *12* (51), 12218−12224.
(26) Cong, X.; Patrick, J. W.; Liu, Y.; Liang, X.; Liu, W.; Laganowsky, A. Investigation of Protein-Lipid Interactions Using Native Mass SpectrometrySpectrometry. In *Microbial Systems Biology: Methods and Protocols*; Navid, A., Ed.; Methods in Molecular Biology; Springer US: New York, NY, 2022; pp 41−64. DOI: 10.1007/978-1-0716-1585-0_3.
(27) Miller, Z. M.; Zhang, J. D.; Donald, W. A.; Prell, J. S. *Anal. Chem.* **2020**, *92* (15), 10365−10374.
(28) Barrera, N. P.; Di Bartolo, N.; Booth, P. J.; Robinson, C. V. *Science* **2008**, *321* (5886), 243−246.
(29) Konijnenberg, A.; van Dyck, J. F.; Kailing, L. L.; Sobott, F. *Biol. Chem.* **2015**, *396* (9−10), 991−1002.
(30) Liu, X.; Golden, L. C.; Lopez, J. A.; Shepherd, T. R.; Yu, L.; Fuentes, E. J. *Biophys. J.* **2019**, *116* (12), 2314−2330.
(31) Naider, F.; Becker, J. M.; Lee, Y.-H.; Horovitz, A. *Biochemistry* **2007**, *46* (11), 3476−3481.
(32) Lyu, J.; Zhang, T.; Marty, M. T.; Clemmer, D.; Russell, D.; Laganowsky, A. Double and Triple Thermodynamic Mutant Cycles

Reveal the Basis for Specific MsbA-Lipid Interactions. *eLife* **2024**, *12*. DOI: 10.7554/eLife.91094.
(33) Fodor, A. A.; Aldrich, R. W. *J. Biol. Chem.* **2004**, *279* (18), 19046−19050.
(34) Vaughan, C. K.; Harryson, P.; Buckle, A. M.; Fersht, A. R. *Acta Crystallogr. D Biol. Crystallogr.* **2002**, *58* (4), 591−600.
(35) Horovitz, A. *Fold. Des.* **1996**, *1* (6), R121−R126.
(36) Carter, P. J.; Winter, G.; Wilkinson, A. J.; Fersht, A. R. *Cell* **1984**, *38* (3), 835−840.
(37) Sokolovski, M.; Cveticanin, J.; Hayoun, D.; Korobko, I.; Sharon, M.; Horovitz, A. *Nat. Commun.* **2017**, *8* (1), 212.
(38) Gianni, S.; Haq, S. R.; Montemiglio, L. C.; Jurgens, M. C.; Engstrom, A.; Chi, C. N.; Brunori, M.; Jemth, P. *J. Biol. Chem.* **2011**, *286* (31), 27167−27175.
(39) Pagano, L.; Toto, A.; Malagrinò, F.; Visconti, L.; Jemth, P.; Gianni, S. *Int. J. Mol. Sci.* **2021**, *22* (2), 828.
(40) Borgnia, M.; Nielsen, S.; Engel, A.; Agre, P. *Annu. Rev. Biochem.* **1999**, *68*, 425−458.
(41) Borgnia, M. J.; Agre, P. *Proc. Natl. Acad. Sci. U. S. A.* **2001**, *98* (5), 2888−2893.
(42) Calamita, G.; Bishai, W. R.; Preston, G. M.; Guggino, W. B.; Agre, P. *J. Biol. Chem.* **1995**, *270* (49), 29063−29066.
(43) Savage, D. F.; Egea, P. F.; Robles-Colmenares, Y.; O'Connell, J. D., III; Stroud, R. M. *PLOS Biol.* **2003**, *1* (3), No. e72.
(44) Schmidt, V.; Sidore, M.; Bechara, C.; Duneau, J.-P.; Sturgis, J. N. *Biochim. Biophys. Acta BBA - Biomembr.* **2019**, *1861* (2), 431−440.
(45) Laganowsky, A.; Reading, E.; Allison, T. M.; Ulmschneider, M. B.; Degiacomi, M. T.; Baldwin, A. J.; Robinson, C. V. *Nature* **2014**, *510* (7503), 172−175.
(46) Schmidt, V.; Sturgis, J. N. *ACS Omega* **2017**, *2* (6), 3017−3027.
(47) Sun, J.; Kitova, E. N.; Wang, W.; Klassen, J. S. *Anal. Chem.* **2006**, *78* (9), 3010−3018.
(48) Wang, W.; Kitova, E. N.; Klassen, J. S. *Anal. Chem.* **2003**, *75* (19), 4945−4955.
(49) Zhang, S.; Van Pelt, C. K.; Wilson, D. B. *Anal. Chem.* **2003**, *75* (13), 3010−3018.
(50) Cockroft, S. L.; Hunter, C. A. *Chem. Soc. Rev.* **2007**, *36* (2), 172−188.
(51) McCabe, J. W.; Shirzadeh, M.; Walker, T. E.; Lin, C.-W.; Jones, B. J.; Wysocki, V. H.; Barondeau, D. P.; Clemmer, D. E.; Laganowsky, A.; Russell, D. H. *Anal. Chem.* **2021**, *93* (18), 6924−6931.
(52) Marty, M. T.; Baldwin, A. J.; Marklund, E. G.; Hochberg, G. K. A.; Benesch, J. L. P.; Robinson, C. V. *Anal. Chem.* **2015**, *87* (8), 4370−4376.
(53) Jiang, J.; Daniels, B. V.; Fu, D. *J. Biol. Chem.* **2006**, *281* (1), 454−460.

https://doi.org/10.1021/acs.analchem.4c01704
Anal. Chem. XXXX, XXX, XXX−XXX